A New Equivalent Network Method for Analyzing Discontinuity Properties of Open Dielectric Waveguides

HIROSHI SHIGESAWA, SENIOR MEMBER, IEEE, AND MIKIO TSUJI, MEMBER, IEEE

Abstract—**A novel network approach is proposed for analyzing interacting discontinuities on open planar dielectric waveguides by accurately taking account of both surface modes and waves with continuous spectra. In our approach, a continuum of the radiation wave is recomposed into a set of the newly defined "spectral composite" modes, each of them carrying a finite magnitude of radiation power, and these new modes, in conjunction with surface modes, construct the complete orthonormal set for expressing an arbitrary local field on a dielectric slab waveguide. This idea allows us to provide the modal voltages and currents of the spectral composite modes in the identical definition with those for the surface modes with discrete eigenvalues, thereby developing an equivalent network approach effective for solving discontinuity problems, even on an open waveguide, with the familiar approach for closed waveguide problems. A number of numerical results are shown to prove the usefulness of our approach.**

I. INTRODUCTION

OPEN DIELECTRIC waveguides have become increasingly important in the past few years, particularly in connection with integrated circuits ranging from millimeter-wave to optical frequencies [1], [2]. In such an open waveguide, however, the discontinuities often give rise to serious problems in circuit performance, and it has recently become necessary to extensively analyze the discontinuity problems with high precision.

In previous papers [3], [4] we described the feature of mode propagation through an isolated step discontinuity from a full-wave analytical point of view, and clarified the behavior of both the radiation field and the surface wave field. Practical circuits, however, usually do not include a discontinuity as an isolated case; rather, they consist of an arbitrary combination of discontinuities connected via the interconnecting homogeneous dielectric waveguides. On such a discontinuous structure, the fields vary with the successive positions along it. Thus it is necessary to consider rigorously the field continuity conditions on the whole boundary surface of the structure by taking into account the effect not only of the conversion of power among the surface modes and the scattering of power into the radiation modes [5] but also of the coupling of the power of the radiation mode into both surface modes and the other radiation modes. However, each of the radiation modes is certainly not an eigenmode like a surface mode characterized by each of the discrete propagation constants, and its power intensity is infinite according to the orthonormal relation expressed by the Dirac delta function. Therefore the scattered and coupled powers mentioned above should be discussed by always considering a continuum of the radiation modes. This fact has been one of the main reasons making it almost impossible to develop a simple and effective equivalent network approach for analyzing open dielectric waveguide problems, although an equivalent network approach is quite familiar to microwave engineers dealing with closed waveguide problems [6].

Now, the functional forms of the modal functions themselves of both surface modes and radiation modes do not change as they propagate along a homogeneous slab waveguide, but their complex amplitude and the continuous spectral amplitude change. The change in the complex amplitude of each of surface modes is easily pictured by the simple network model consisting of uncoupled, parallel transmission lines, even for a slab waveguide of the open type. Contrary to this, it is almost impossible to picture the change in the continuous spectral amplitude of radiation modes in the same fashion as the surface modes, and, as an intermediate step, it is natural to expand the varying continuous spectral function into a discrete sequence of functions belonging to a complete set. As will be shown below, this idea makes it possible to overcome the difficulty mentioned previously. A similar expression appeared in [7] and [8] in connection with an isolated step discontinuity, but problems of its combination were not discussed at all.

On the other hand, Rozzi *et al.* [9] expanded not the varying spectral function, but the nonvarying modal functions into a discrete sequence of the complete function defined in the coordinate space. This approach, therefore, leaves the radiation mode still in the form of a continuum, and their idea does not basically release us from the difficulty of developing a simple equivalent network.

Manuscript received February 26, 1987; revised July 8, 1988. This work was supported by the Ministry of Education, Science and Culture of Japan under a Grant-in-Aid for General Scientific Research and by a research grant from the Mazda Foundation.

The authors are with the Department of Electronics, Doshisha University, Karasuma-Imadegawa, Kamikyo-ku, Kyoto, 602 Japan.

IEEE Log Number 8824249.

0018-9480/89/0100-0003$01.00 ©1989 IEEE

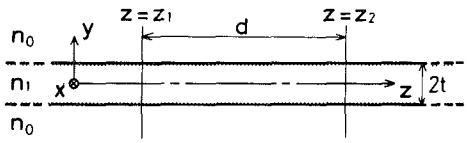

Fig. 1. Planar dielectric waveguide uniform in the x direction.

This paper initiates a breakthrough in surmounting this difficulty. Our idea certainly is based on the expansion of the continuous spectral amplitude, but we recompose it to have a discrete set of an infinite number of newly defined "spectral composite" modes [10], which construct the complete orthonormal set for expressing an arbitrary local field in conjunction with the surface modes. It is also proved that each of the spectral composite modes carries a finite magnitude of radiation power according to the orthonormal relation expressed not by the Dirac delta function, but by the Kronecker delta symbol, such as the surface modes. This means that the terminal parameters (root power amplitude, wave impedance, etc.) of the equivalent network for the spectral composite modes can be defined identically with those for the surface modes, and we can allocate the discrete terminal ports to each of the two types of mode. As a result, our approach, unlike Rozzi's, can treat independently each of the isolated step discontinuities and the interconnecting homogeneous slab waveguides as a building block in a usual equivalent network.

After explaining briefly our idea and developing a mathematical formulation in Section II, the effectiveness of our approach will be demonstrated by comparing it with published results in Section III-A. These results are then applied to discuss the wave behavior along dielectric corrugations of finite extent on slab waveguides of the open type in Section III-B.

II. General Approach

A. Homogeneous Dielectric Waveguide and Spectral Composite Mode

To make our idea clear, we first consider a homogeneous dielectric slab waveguide of the type shown in Fig. 1. We assume here that M surface modes and the radiation modes polarized in the x direction are traveling to the positive z direction. Let $e_{xj}(y)$, $h_{yj}(y)$ and $e_x(y,\rho)$, $h_y(y,\rho)$ be the orthonormal modal functions of the jth surface mode and the radiation mode, respectively (see [5] for their functional forms). Here ρ denotes the transverse wavenumber of the radiation mode in the y direction outside the slab. Each type of modal function is normalized in terms of the Kronecker delta symbol or Dirac delta function as noted in [5, sec. 8.5]. Although the wavenumber ρ covers all of the values from 0 to ∞, the radiation modes in the range $0 \leqslant \rho \leqslant n_0 k_0$ are propagating into the z direction, while those in the range $n_0 k_0 \leqslant \rho < \infty$ are nonpropagating. Therefore, the total electric field $E_x(y, z_1)$ on the plane at $z = z_1$ is completely expressed[1] by the following equation [5]:

$$E_x(y,z_1) = \sum_{m=0}^{M-1} A_m(z_1) e_{xm}(y) + \int_0^{n_0k_0} f(\rho,z_1) e_x(y,\rho)\, d\rho + \int_{n_0k_0}^{\alpha n_0k_0} g(\rho,z_1) e_x(y,\rho)\, d\rho \qquad (1)$$

where $f(\rho, z_1)$ and $g(\rho, z_1)$ are the continuous spectral functions for the radiation modes at $z = z_1$ and the coefficients $A_m(z_1)$ stand for the root-power amplitude of the surface modes.

Now, the electric field of (1) after propagating to the plane at $z = z_2 (> z_1$ with $d = z_2 - z_1)$ can be written as follows:

$$E_x(y,z_2) = \sum_{m=0}^{M-1} B_m(z_2) e_{xm}(y) + \int_0^{n_0k_0} f(\rho,z_2) e_x(y,\rho)\, d\rho + \int_{n_0k_0}^{\alpha n_0k_0} g(\rho,z_2) e_x(y,\rho)\, d\rho \qquad (2)$$

where

$$B_m(z_2) = A_m(z_1)\exp(-j\beta_m d)$$
$$f(\rho,z_2) = f(\rho,z_1)\exp(-j\beta(\rho)d)$$
$$g(\rho,z_2) = g(\rho,z_1)\exp(-\gamma(\rho)d). \qquad (3)$$

β_m is the phase constant of the mth surface mode, while $\beta(\rho) = \sqrt{(n_0k_0)^2 - \rho^2}$ and $\beta(\rho) = -j\sqrt{\rho^2 - (n_0k_0)^2} = -j\gamma(\rho)$ are the phase constants of the propagating and the nonpropagating radiation modes, respectively.

The modal functions of both surface modes and radiation modes in (1) and (2) do not change as they propagate along the guide axis. Then, there is a one-to-one correspondence between $A_m(z_1)$ and $B_m(z_2)$ for each surface mode. The constitutive component of $E_x(y, z_2)$ corresponding to the radiation mode, shown by the branch-cut integral in (2), varies in its resultant functional form along the y axis as the radiation mode propagates the distance d, although the amplitudes of the spectral functions $f(\rho, z_2)$ and $g(\rho, z_2)$ are simply related to $f(\rho, z_1)$ and $g(\rho, z_1)$, respectively, through (3).

Our motivation here is to express such a varying field by a similar expansion form with the surface wave field as seen in the first term of the right-hand side of (2). To this end, recalling $e_x(y, \rho)$ to be independent of z, it is quite natural to expand $f(\rho, z_1)$ and $g(\rho, z_1)$ into a complete set of the orthonormal functions $\phi_n(\rho)$ and $\psi_n(\rho)$ of only ρ as

[1]For practical calculations, the upper limit of the second integral is replaced by an optimally scaled limit given by $\alpha n_0 k_0$, where $\alpha > 1$ (see [4] for details).

follows:

$$f(\rho, z_1) = \sum_{n=0}^{N-1} A_{M+n}(z_1)\phi_n(\rho)$$

$$g(\rho, z_1) = \sum_{n=0}^{N-1} A_{M+N+n}(z_1)\psi_n(\rho) \tag{4}$$

where

$$\int_0^{n_0k_0} \phi_m(\rho)\phi_n(\rho)\, d\rho = \delta_{mn}$$

$$\int_{n_0k_0}^{\alpha n_0k_0} \psi_m(\rho)\psi_n(\rho)\, d\rho = \delta_{mn}. \tag{5}$$

Similar expansions hold for the spectral functions $f(\rho, z_2)$ and $g(\rho, z_2)$ by replacing $A_{M+n}(z_1)$ and $A_{M+N+n}(z_1)$ in (4) with $B_{M+n}(z_2)$ and $B_{M+N+n}(z_2)$, respectively.

Here, it should be noted that the expansion coefficients $A_i(z)$ and $B_i(z)$ are still functions of z because the continuous spectral functions deform as the radiation modes propagate along the guide. We advance further the expansions of (4) to obtain a discrete set of an infinite number of what are being called spectral composite modes, defined by

$$\tilde{e}_{xn}(y) = \int_0^{n_0k_0} \phi_n(\rho)e_x(y, \rho)\, d\rho$$

$$\hat{e}_{xn}(y) = \int_{n_0k_0}^{\alpha n_0k_0} \psi_n(\rho)e_x(y, \rho)\, d\rho. \tag{6}$$

It is easily proved that these spectral composite modes have orthonormal relations subject not to the Dirac delta function but to the Kronecker delta symbol (see Appendix I). Substituting (4) into (3) and applying the definition of (6), (1) and (2) can be reduced to the forms

$$E_x(y, z_1) = \sum_{m=0}^{M-1} A_m(z_1)e_{xm}(y) + \sum_{n=0}^{N-1} [A_{M+n}(z_1)\tilde{e}_{xn}(y) + A_{M+N+n}(z_1)\hat{e}_{xn}(y)] \tag{7}$$

$$E_x(y, z_2) = \sum_{m=0}^{M-1} B_m(z_2)e_{xm}(y) + \sum_{n=0}^{N-1} [B_{M+n}(z_2)\tilde{e}_{xn}(y) + B_{M+N+n}(z_2)\hat{e}_{xn}(y)]. \tag{8}$$

Since the modal functions of all modes in (7) and (8) are now subject to the orthonormal relation expressed by the Kronecker delta symbol, we can picture the simple terminal model for the equivalent network of a homogeneous dielectric waveguide at least at the local position at $z = z_1$ or z_2; one of the terminal ports can be allocated to each of the two spectral composite modes and surface modes. However, the amplitude, for example, $A_{M+n}(z_1)$, of the spectral composite mode changes in its magnitude as well as in its phase as it propagates. Such a difference in magnitudes between two positions at $z = z_1$ and z_2 reminds us that there is no longer a one-to-one correspondence between A_{M+n} and B_{M+n} or A_{M+N+n} and B_{M+N+n}, and one of the input spectral composite modes at $z = z_1$

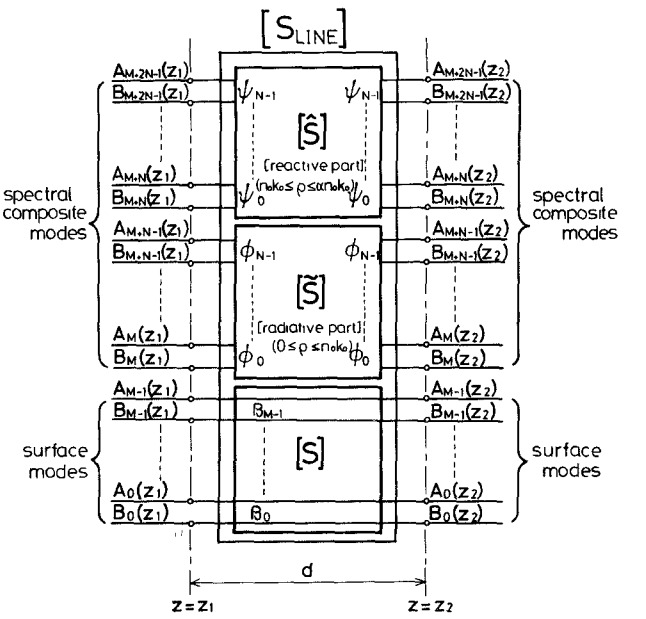

Fig. 2. Equivalent network representation for the homogeneous slab waveguide, where the spectral composite modes are introduced by using the complete orthonormal functions ϕ_n and ψ_n defined in each range of ρ indicated in the network $[\tilde{S}]$ and $[\hat{S}]$, respectively.

necessarily couples to all of the output spectral composite modes at $z = z_2$ while it propagates. Let us then substitute $f(\rho, z_1)$ of (4) into that of (3) to obtain

$$\sum_{n=0}^{N-1} B_{M+n}(z_2)\phi_n(\rho) = \sum_{k=0}^{N-1} A_{M+k}(z_1)\phi_k(\rho)\exp(-j\beta(\rho)d) \tag{9}$$

where the coefficients $A_q(z_i)$ and $B_q(z_i)$ are defined so as to stand for the root-power amplitudes of the spectral composite mode. By using the orthonormal relation of $\phi_n(\rho)$, we have

$$B_{M+n}(z_2) = \sum_{k=0}^{N-1} \tilde{S}_{nk}A_{M+k}(z_1) \tag{10}$$

where

$$\tilde{S}_{nk} = \int_0^{n_0k_0} \phi_n(\rho)\phi_k(\rho)\exp(-j\beta(\rho)d)\, d\rho. \tag{11}$$

By following the same method we have

$$B_{M+N+n}(z_2) = \sum_{k=0}^{N-1} \hat{S}_{nk}A_{M+N+k}(z_1) \tag{12}$$

where

$$\hat{S}_{nk} = \int_{n_0k_0}^{\alpha n_0k_0} \psi_n(\rho)\psi_k(\rho)\exp(-\gamma(\rho)d)\, d\rho. \tag{13}$$

If any field distribution given at $z = z_2$ propagates to the negative z direction, the resultant field at $z = z_1$ can be expressed by relations similar to (10) and (12). As a result, the equivalent network for a homogeneous dielectric waveguide of length d can be represented by Fig. 2 and the terminal amplitudes are governed by the matrix $[S_{\text{LINE}}]$

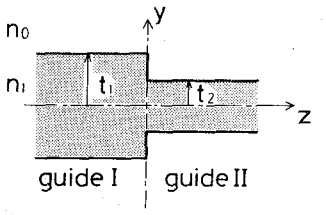

Fig. 3. Step discontinuity configuration in planar dielectric waveguides.

given in Appendix II. We believe that the formulation described there, although seen to be a familiar expression on the surface, is unprecedented because it makes it possible to analyze the problems of interacting discontinuities on open waveguides by the network approach that is well developed for the problems in closed waveguides.

B. Step Discontinuity

Let us next derive the equivalent network for a step discontinuity between two semi-infinite homogeneous waveguides I and II with different thicknesses as shown in Fig. 3. According to the asymmetry of such a structure with respect to the junction plane, we should consider one more type of step discontinuity, which is merely inverted with respect to the plane of Fig. 3. First, we consider that one of modes is incident normally to the step from the left-hand side or the right-hand side of Fig. 3. An example of such cases of excitation is the incidence of the qth surface mode from the left-hand side. Then, the electric fields tangential to the discontinuity plane at $z = 0$ can be expressed as follows [4]:

$$E_x^{\mathrm{I}}(y,0^-) = \sum_{p=0}^{M+2N-1} (\delta_{qp} + R_{qp}) e_{xp}^{\mathrm{I}}(y) \qquad (14)$$

$$E_x^{\mathrm{II}}(y,0^+) = \sum_{p=0}^{M+2N-1} T_{qp} e_{xp}^{\mathrm{II}}(y) \qquad (15)$$

where

$$\begin{aligned} e_{xp}^{i}(y) &= e_{xm}^{i}(y) \qquad \text{for } p = 0,1,\cdots,M-1 \qquad (m = p) \\ &= \tilde{e}_{xn}^{i}(y) \qquad \text{for } p = M,\cdots,M+N-1 \\ &\qquad\qquad (n = p - M) \\ &= \hat{e}_{xn}^{i}(y) \qquad \text{for } p = M+N,\cdots,M+2N-1 \\ &\qquad\qquad (n = p - M - N) \\ &\qquad (i = \mathrm{I} \text{ or } \mathrm{II}). \end{aligned} \qquad (16)$$

R_{qp} and T_{qp} are the unknown coefficients to be determined. We use here the mode-matching method to fit the boundary condition on the plane $z = 0$ in the sense of least mean squares [4], [8], which considers the error ϵ given by the following equation:

$$\epsilon = \frac{1}{2} \cdot \left(\frac{\int_{-\infty}^{\infty} |E_x^{\mathrm{I}} - E_x^{\mathrm{II}}|^2 \, dy}{\int_{-\infty}^{\infty} |e_{xq}^{\mathrm{I}}|^2 \, dy} + \frac{\int_{-\infty}^{\infty} |H_y^{\mathrm{I}} - H_y^{\mathrm{II}}|^2 \, dy}{\int_{-\infty}^{\infty} |h_{yq}^{\mathrm{I}}|^2 \, dy} \right) \qquad (17)$$

where H_y^{I} and H_y^{II} are the magnetic fields associated with the electric fields of (14) and (15), respectively, and e_{xq}^{I} and h_{yq}^{I} are the electric and magnetic fields of the incident mode.

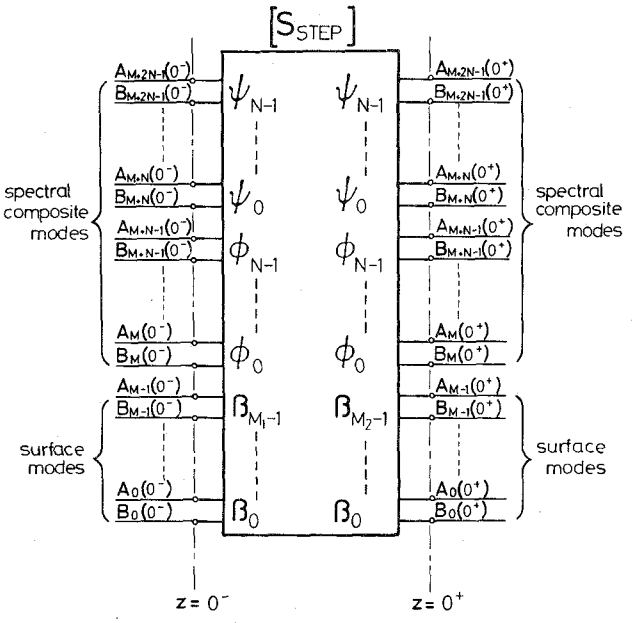

Fig. 4. Equivalent network representation for the step discontinuity shown in Fig. 3.

Minimizing ϵ with respect to the unknowns by the procedures described in [4], we can easily solve them. Applying the same procedure to all of the other excitation cases, one can obtain all of the unknown coefficients R_{qp} and T_{qp} which are linked with the elements of the matrix $[S_{\mathrm{STEP}}]$ representing the isolated step discontinuity, as mentioned in Appendix III. As a result, a step discontinuity can be expressed by the equivalent network of Fig. 4, which again has the terminal ports corresponding to each of the two surface modes and spectral composite modes. By following the same procedures, we can derive one more matrix, $[S'_{\mathrm{STEP}}]$, for the step discontinuity, whose structure is the inversion of Fig. 3 with respect to the $x-y$ plane at $z = 0$.

Here it is necessary to comment on a reasonable choice for a set of expansion functions in (4). The spectral composite modes of our definition are based on the expansion of the continuous spectral function partitioned into two finite ranges on the wavenumber (ρ) plane, and they are applied to the mode-matching method in the form of (17). This problem is mathematically the best approximation calculation based on the unweighted L^2 norm in the finite range of variables, so that Legendre polynomials are the best basis functions [11], [12]. Therefore, we will use them in the following section.

III. Propagation Characteristics of Modes Along Practical Structures

A. Mode Propagation Through Symmetric Double Step

We first discuss the symmetric double step shown in Figs. 5 and 6. These structures play an important role in practical planar circuits. For example, Fig. 5 appears as a

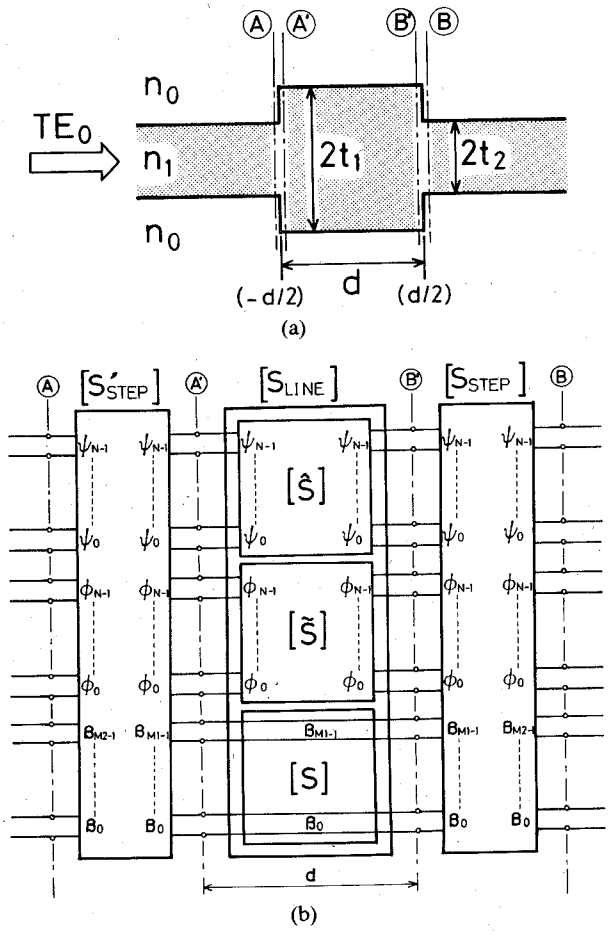

Fig. 5. Symmetric double-step discontinuity: (a) the configuration on the longitudinal section and (b) its equivalent network. The networks $[\tilde{S}]$ and $[\hat{S}]$ represent the coupling effect between the spectral composite modes in each range of ρ.

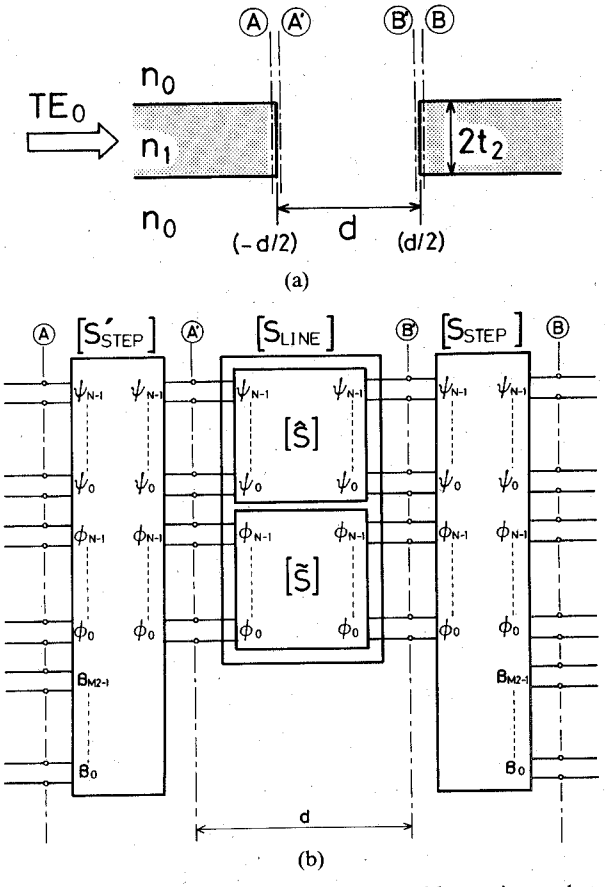

Fig. 6. Symmetric double-step discontinuity with an air gap between two planar dielectric waveguides: (a) the configuration on the longitudinal section and (b) its equivalent network.

constitutive block of dielectric grating filters [13], while Fig. 6 often appears as the coupling section of planar dielectric resonators [14]. We assume that the guide with a thickness $2t_1$ in the case of Fig. 5 supports M_1 surface modes, while the guide with thickness $2t_2$ in the case of both Fig. 5 and Fig. 6 supports M_2 surface modes. The structure of Fig. 5(a) is partitioned into three building blocks by correctly defining the terminal planes as shown. They are two step discontinuities and one homogeneous waveguide of length d interconnecting the two interacting steps. Introducing the equivalent networks $[S_{\text{STEP}}]$, $[S_{\text{LINE}}]$, and $[S_{\text{STEP}}]$ of Figs. 2 and 4, the complete equivalent network can be expressed as shown in Fig. 5(b). When the TE_0 fundamental surface mode is the only mode incident from the left-hand side of the structure (as shown), all of the terminal ports, except for the input port of the incident surface mode, should be terminated properly by the corresponding characteristic impedance of the equivalent transmission lines for each surface mode or by the matched termination impedance for each spectral composite mode (see Appendix IV). As a result, we can obtain the complete equivalent network for the structure as shown in Fig. 5(b).

On the other hand, the double step of Fig. 6(a) is an air gap between terminal planes (A') and (B'), so the equivalent network for this gap is expressed in terms of only the spectral composite modes. Therefore, by taking away the equivalent transmission lines for the surface modes interconnecting planes A' and B' in Fig. 5(b), we have the complete equivalent network for Fig. 6(a), as shown in Fig. 6(b).

Now, assuming the incident TE_0 surface mode with unit root power amplitude in both Figs. 5(b) and 6(b), one can straightforwardly obtain $B_{N1+n}(-d/2)$ and $B_{N1+n}(d/2)$ for the nth spectral composite mode at planes (A) and (B), respectively, as well as $B_m(-d/2)$ and $B_m(d/2)$ of the reflected and transmitted surface modes, respectively. These amplitudes give the total electric field at planes (A) and (B) through (7) and (8). If the steepest descent path (SDP) approximation is applied to the first term in the bracket of (7) and (8) expressing the spectral composite modes of the radiative part, we can calculate the fields radiated in both the forward $(+z)$ and backward $(-z)$ directions.

Numerical examples are obtained for the double step with the dimension indicated in the insets of Figs. 7 and 8. For the given values of the parameters, only the TE_0 fundamental surface mode can propagate in the dielectric waveguide with thickness $2t_2$, while the waveguide of thickness $2t_1$ in Fig. 7 supports the TE_0 and TE_2 modes. The reflection coefficient R_0 and the transmission coeffi-

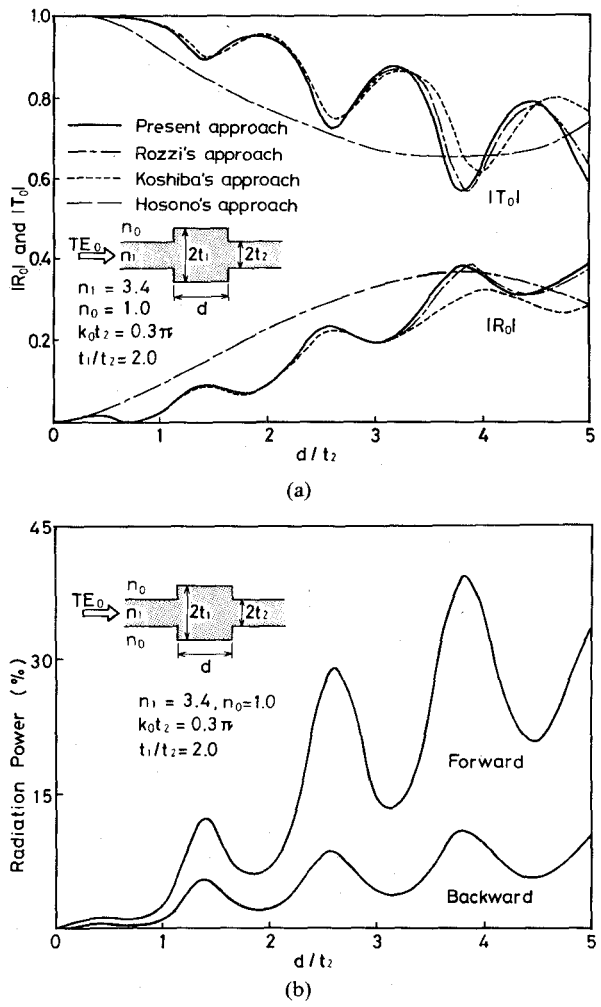

Fig. 7. Numerical results of symmetric double-step: (a) reflection and transmission coefficients, and (b) radiation powers versus the rib width.

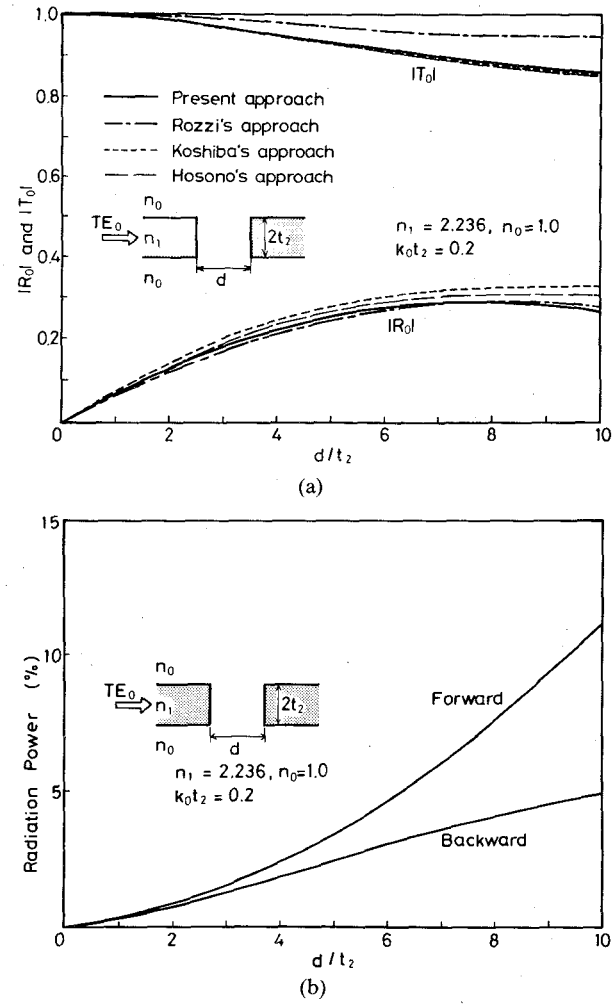

Fig. 8. Numerical results of symmetric double-step with an air gap: (a) reflection and transmission coefficients, and (b) radiation powers versus the gap width.

cient T_0 of the surface mode are shown in Figs. 7(a) and 8(a), while the backward and forward radiation powers are shown in (b) as a function of the relative length h/t_2. The results indicated by the solid curves are calculated by using a scale factor of $\alpha = 7$ and by taking the expansion terms of the Legendre function as $N = 9$ (satisfactory convergence of solutions has already been confirmed in [4]). The results for only R_0 and T_0 can be compared with those calculated by Rozzi *et al.* [9], Koshiba *et al.* [15], and Hosono *et al.* [16]. Koshiba's approach introduces a perfectly conducting boundary away from the guide surface and applies the finite element method to the limited region around the discontinuities. Hosono's approach replaces the original unbounded configuration by a corresponding periodic multilayer structure instead of a conducting boundary as seen in Koshiba's approach. As for Fig. 7(a), Hosono's results are in good agreement with ours, but Koshiba's results disagree for $d/t_2 > 3.5$. Such a discrepancy, as asserted in their own paper [15], is due to the insufficient number of elements for the rib region in the calculations.

On the other hand, Rozzi's results show a very different feature from those seen in other three results. As noted in [16], the rib region behaves almost like a low-Q resonator. Then, R_0 and T_0 may oscillate for the range of about $d > \lambda_0/(2n_1)$ (i.e., $d/t_2 = 0.98$), while Rozzi's results do not. As for Fig. 8(a), our results for T_0 agree quite well with those obtained by Hosono *et al.*, and Koshiba *et al.*, but disagree with Rozzi's results. Contrary to this, the computed values of R_0 exhibit a small amount of the difference between the results obtained by these approaches.

For a more precise comparison, the radiation power must be determined, but our method is only one that calculates it. Our results, shown in Fig. 7(b), exhibit an oscillatory nature corresponding to that seen in Fig. 7(a), and the radiation maxima just coincide with the oscillation maxima of R_0 and the minima of T_0 in our results. On the other hand, the radiation powers shown in Fig. 8(b) monotonically increase with increasing d/t_2, corresponding to similar features of R_0 and T_0 in Fig. 8(a). Incidentally, the calculations presented here have been made with an error of about 0.5 percent or less in the power conservation relation at around $d/t_2 = 10$.

Koshiba's and Hosono's approaches essentially alter the actual boundary condition for the radiation field. This is a

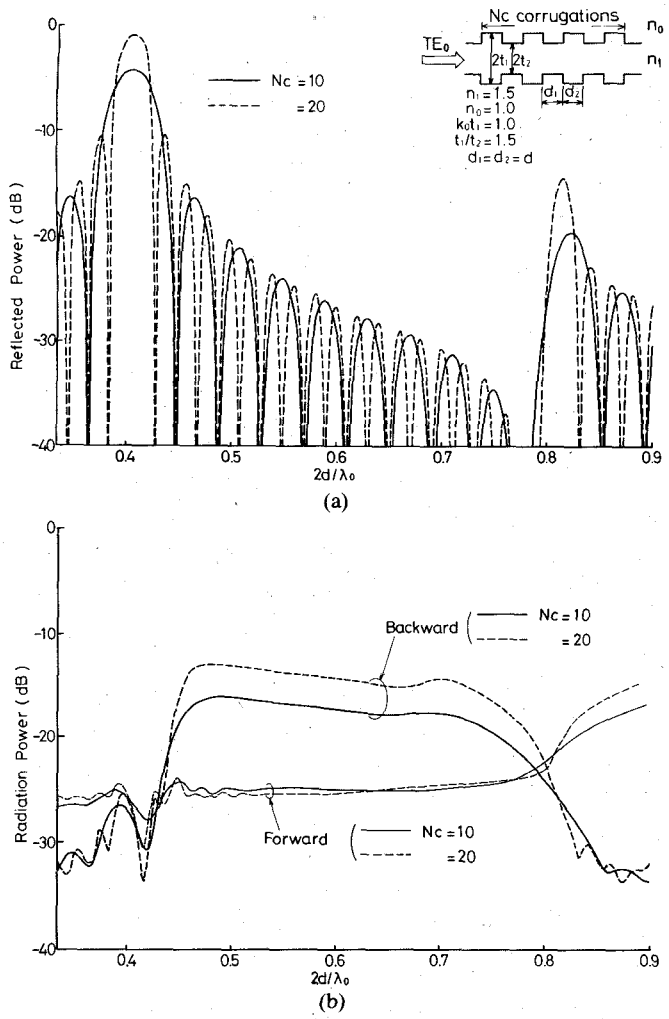

Fig. 9. Numerical results for the periodic structure with a finite number N_c of corrugations: (a) reflected power of the incident TE_0 mode and (b) radiation powers versus the normalized period $2d/\lambda_0$.

serious drawback in practical applications because such approximations make it absolutely impossible to obtain any information about the real fields scattered and/or radiated from the discontinuities into the space outside the original structures of the open type.

B. Mode Propagation Through Periodic Corrugations with Finite Length

Let us next consider the periodic dielectric corrugations of finite length as shown in the inset of Fig. 9(a). This structure is given by the cascade connection of a finite number of networks given by Figs. 2 and 4, and we can derive the final equivalent network for Fig. 9 by connecting repeatedly such constitutive networks expressed by the matrices $[S_{STEP}]$, $[S'_{STEP}]$, and $[S_{LINE}]$. Applying the calculation procedures mentioned above in subsection A, we can obtain the numerical results shown in Fig. 9. These examples are obtained for a structure with the dimensions indicated in the inset and for a different number N_c of corrugations. The only surface mode propagating in each homogeneous waveguide section is the TE_0 fundamental mode and we consider that this mode incident from the

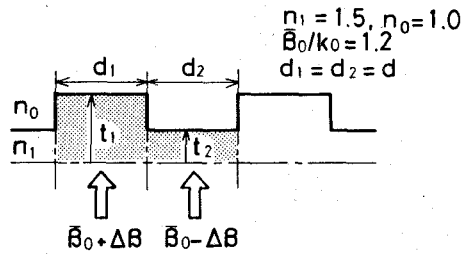

Fig. 10. Unit cell composing the periodic structure with an almost invariable phase constant $\bar{\beta}_0$. The guides with thickness $2t_1$ and $2t_2$ (though the figure shows its half section) have the phase constants $\bar{\beta}_0 + \Delta\beta$ and $\bar{\beta}_0 - \Delta\beta$, respectively.

left-hand side excites the structure. Fig. 9(a) shows the reflected power of the TE_0 surface mode in the case where $N_c = 10$ and 20 corrugations, as a function of the normalized period $2d/\lambda_0$, while Fig. 9(b) shows the forward and backward radiation powers. If the structure under consideration is infinite in length, the first Bragg reflection occurs in the limited range of $2d/\lambda_0$ between 0.398 and 0.414, while the power radiation into space occurs only in the leaky wave region beyond $2d/\lambda_0 = 0.448$ for the present case. As seen from Fig. 9(a), it is found that strong reflection indeed appears at around $2d/\lambda_0 = 0.406$, corresponding to the center frequency of the first Bragg reflection region and also that significant radiation occurs in the leaky wave region. However there are many subsidiary reflection peaks of the surface mode even outside the first Bragg reflection region, and the radiation still occurs in the first Bragg reflection region with a complicated feature arising from the finite length of the periodic structure.

Since a residual loss in the Bragg reflection region often has a significant effect on the grating filter performance, let us consider the cause of it for several kinds of structures, whose dimensions are chosen so that maximum reflection occurs at nearly the same mid-stopband frequency, even for different ratios t_1/t_2. To have such structures, we consider one section of corrugations as shown in Fig. 10. The constitutive subsections, with thicknesses $2t_1$ and $2t_2$, have the phase constants $\bar{\beta}_0 + \Delta\beta$ and $\bar{\beta}_0 - \Delta\beta$ at the mid-stopband frequency, respectively. Then, assuming $d_1 = d_2$, the average phase constant over one section may be approximated by $\bar{\beta}_0$; hence the condition to keep $\bar{\beta}_0$ constant gives a necessary pair of guide thicknesses t_1 and t_2 through the characteristic equation of a slab waveguide. An example for $\bar{\beta}_0/k_0 = 1.2$ and $n_1 = 1.5$ is shown in Fig. 11 as a function of the $\Delta\beta/k_0$ value, from which we select two kinds of typical examples to be discussed below. One is the structure with a weak discontinuity, corresponding to $\Delta\beta/k_0 = 0.04$ ($t_1/t_2 = 1.46$), and the other is that with a rather strong discontinuity, corresponding to $\Delta\beta/k_0 = 1.2$ ($t_1/t_2 = 3.44$). Fig. 12 shows the numerical results of the reflection power of the TE_0 surface mode and the radiation powers in both the forward and the backward direction calculated at and near the mid-stopband frequency. It is found that the behavior of the reflection and radiation powers is very complicated owing to the effect of the finite length of the structures.

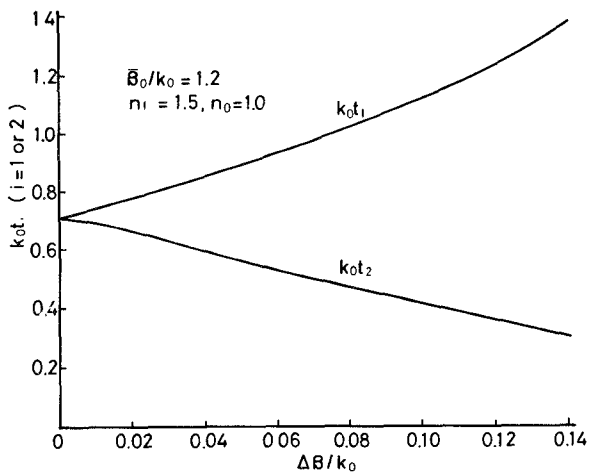

Fig. 11. Paired guide thicknesses for keeping $\bar{\beta}_0$ invariable ($\bar{\beta}_0/k_0 = 1.2$).

However, the mid-stopband insertion loss simply varies as t_1/t_2, as shown in Fig. 13. In the case of Fig. 12(b), the mid-stopband insertion loss attains a value of about 30 dB for $N_c = 20$, as seen in Fig. 13. If this insertion loss is converted into the reflection loss of the surface wave mode only, it becomes 0.0043 dB. As seen from Fig. 12(b), however, the actual reflection loss at the mid-stopband frequency is as much as 0.5 dB, so that we may conclude that the reflection loss is predominantly due to the forward and backward radiation powers. The solid curves in Figs. 14 and 15 show the maximum value of the radiation power within the stopband region for different values of N_c as a function of t_1/t_2. It is found that the radiation power in each direction remains at its extreme value when N_c becomes large.

To estimate approximately this extreme value, the forward radiation power is calculated when the TE_0 surface mode is incident to the isolated step from the $-z$ direction, as shown by the inset of Fig. 14, and the result is shown by the dotted curve. On the other hand, since almost all of the power of the incident surface mode returns to the input port at the mid-stopband frequency, we may estimate the backward radiation power for the original problem by the forward radiation power when the surface mode is incident on the isolated step from the $+z$ direction, as shown in the inset of Fig. 15. The result is also shown by the dotted curve. The approximate numerical results, especially of Fig. 15, show a fairly good agreement with the solid curves, and we may conclude that the residual reflection loss is primarily due to the radiation power produced at the first step discontinuity of the periodic structure when N_c is large. This is a simple but important result for designing grating filters, antennas, etc., but a further discussion of this will be the subject of another paper [17].

Now, as is obvious in Fig. 9(b), the predominant radiation occurs in the backward direction, and the radiation patterns calculated by the SDP approximation are shown in Fig. 16 for structures with $2d/\lambda_0 = 0.477$, 0.516, and 0.577 in the case where $N_c = 10$ and 20. The peak value is normalized to unity for each radiation pattern, and the axes along $\theta = 0°$ and 90° coincide with the y and the negative z directions, respectively. The effect of the finite length is indeed clearly seen in the narrowing main lobe as the number of corrugations increases, but more significantly, such an effect results in complicated spurious lobes. However, the direction of each maximum lobe is in good agreement with the angle calculated from the -1st order space harmonic wave in the structure extending infinitely ($\theta_{\max} = 30°$ for Fig. 16(a), 45° for (b), and 60° for (c)).

IV. Conclusions

We have shown here a new equivalent network approach which is powerful for analyzing the discontinuity problems in open dielectric slab waveguides. Numerical examples have shown our results to be reasonable. One involved a comparative discussion of the interacting double steps; another considered the effect of the finite length of the periodic structures on their propagation and radiation characteristics.

In this paper, we have mainly discussed the guided-wave problems on discontinuous waveguides of the open type. However, the novel network method developed here can easily be applied to other important electromagnetic wave problems, for example, dielectric grating leaky wave antennas and wave scattering problems of dielectric and metal gratings of finite extent. Detailed discussions of them have already been presented in [18]–[20].

Appendix I

Let $\tilde{h}_{yk}(y)$ be the magnetic modal function associated with $\tilde{e}_{xk}(y)$. Then, the orthonormal relations for the spectral composite modes are given as follows.

A. Relations Between the Spectral Composite Modes Belonging to the Same Region of ρ

$$\begin{aligned}
&\int_{-\infty}^{\infty} \tilde{e}_{xn}(y)\tilde{h}_{yk}(y)\,dy \\
&\quad = \int_{-\infty}^{\infty} \left\{ \int_0^{n_0k_0} \phi_n(\rho) e_x(y,\rho)\,d\rho \right\} \\
&\qquad \cdot \left\{ \int_0^{n_0k_0} \phi_k(\rho') h_y(y,\rho')\,d\rho' \right\} dy \\
&\quad = \int_0^{n_0k_0} \int_0^{n_0k_0} \phi_n(\rho)\phi_k(\rho') \\
&\qquad \cdot \left\{ \int_{-\infty}^{\infty} e_x(y,\rho) h_y(y,\rho')\,dy \right\} d\rho\,d\rho' \\
&\quad = \int_0^{n_0k_0} \phi_k(\rho') \left\{ \int_0^{n_0k_0} \phi_n(\rho)\delta(\rho-\rho')\,d\rho \right\} d\rho' \\
&\quad = \int_0^{n_0k_0} \phi_n(\rho')\phi_k(\rho')\,d\rho' = \delta_{nk}. \qquad \text{(A1)}
\end{aligned}$$

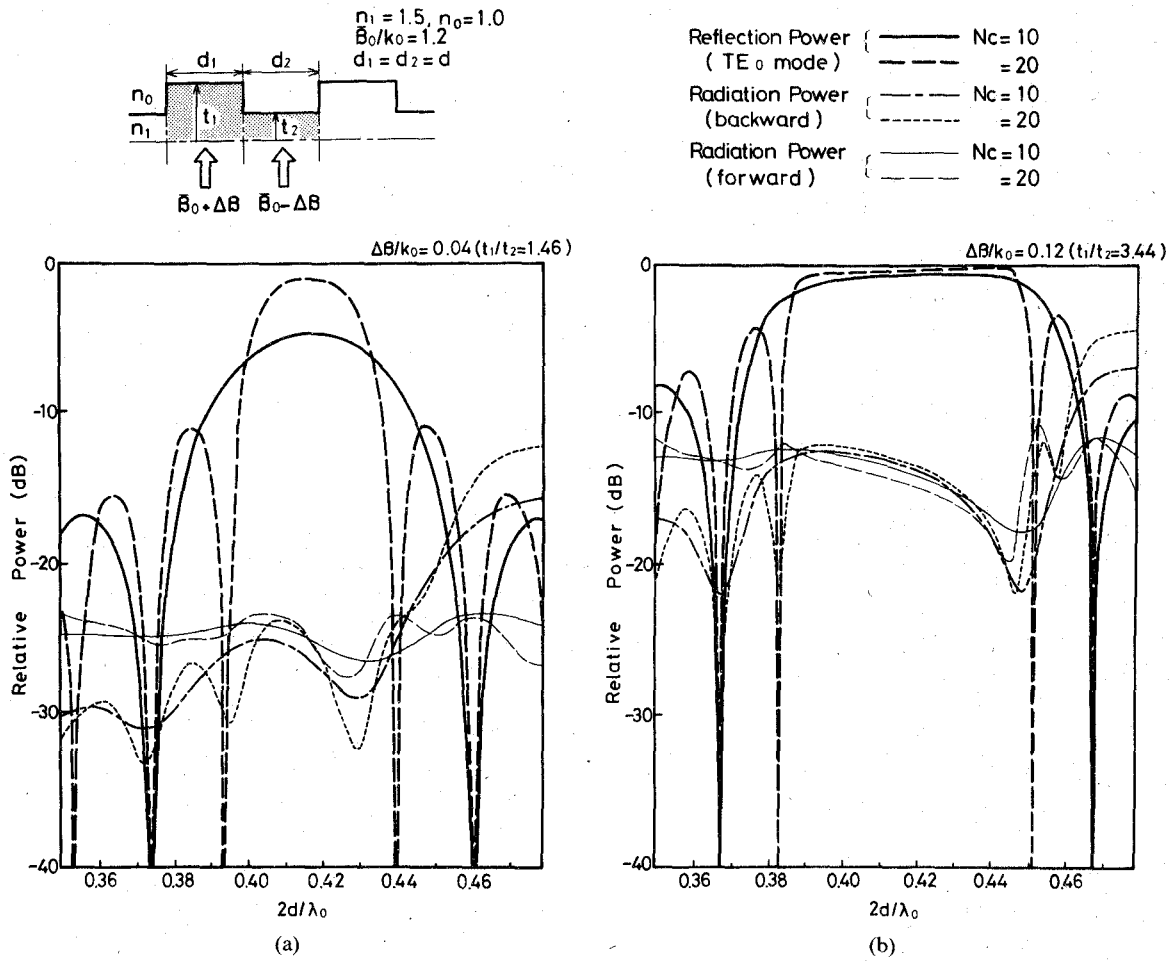

Fig. 12. Reflection and radiation powers for different number of corrugations N_c: (a) weak discontinuity case ($\Delta\beta/k_0 = 0.04$, i.e., $t_1/t_2 = 1.46$), and (b) strong discontinuity case ($\Delta\beta/k_0 = 0.12$, i.e., $t_1/t_2 = 3.44$).

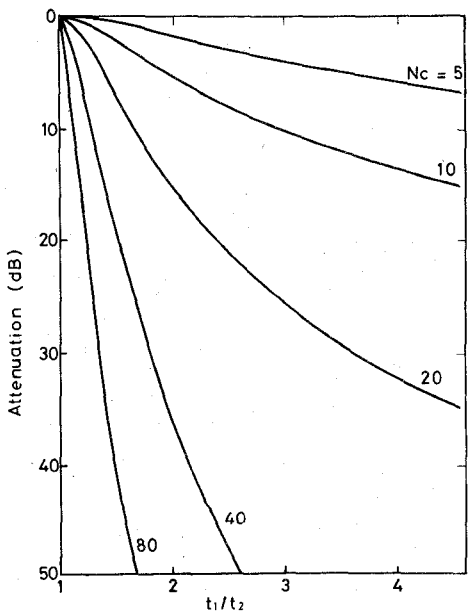

Fig. 13. Mid-stopband insertion loss as a function of the thickness ratio t_1/t_2 of two slab waveguides.

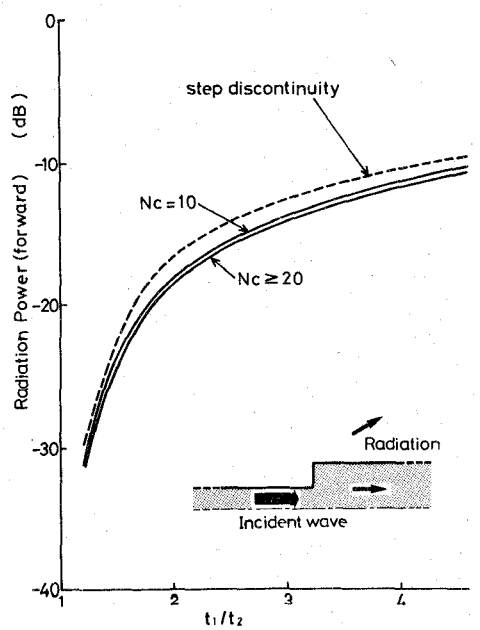

Fig. 14. Maximum forward radiation powers observed within the stopband region. The solid curves are the results obtained by the present method for the periodic structure with a finite number of corrugations N_c, while the dotted curve indicates the radiation power obtained for the step discontinuity shown in the inset.

B. Relations Between the Spectral Composite Modes Belonging to Different Regions of ρ

$$\begin{aligned}\int_{-\infty}^{\infty} \tilde{e}_{xn}(y)\hat{h}_{yk}(y)\,dy &= \int_{-\infty}^{\infty}\left\{\int_0^{n_0k_0}\phi_n(\rho)e_x(y,\rho)\,d\rho\right\}\\ &\quad\cdot\left\{\int_{n_0k_0}^{\alpha n_0k_0}\psi_k(\rho')h_y(y,\rho')\,d\rho'\right\}dy\\ &= \int_{n_0k_0}^{\alpha n_0k_0}\int_0^{n_0k_0}\psi_k(\rho')\phi_n(\rho)\\ &\quad\cdot\left\{\int_{-\infty}^{\infty}e_x(y,\rho)h_y(y,\rho')\,dy\right\}d\rho\,d\rho\\ &= \int_{n_0k_0}^{\alpha n_0k_0}\psi_k(\rho')\left\{\int_0^{n_0k_0}\phi_n(\rho)\delta(\rho-\rho')\,d\rho\right\}d\rho' = 0.\end{aligned} \tag{A2}$$

C. Relations Between a Spectral Composite Mode and a Surface Mode

$$\begin{aligned}\int_{-\infty}^{\infty}\tilde{e}_{xn}(y)h_{ym}(y)\,dy &= \int_{-\infty}^{\infty}\left\{\int_0^{n_0k_0}\phi_n(\rho)e_x(y,\rho)\,d\rho\right\}h_{ym}(y)\,dy\\ &= \int_0^{n_0k_0}\phi_n(\rho)\left\{\int_{-\infty}^{\infty}e_x(y,\rho)h_{ym}(y)\,dy\right\}d\rho = 0.\end{aligned} \tag{A3}$$

APPENDIX II

The equivalent network of Fig. 2 for a homogeneous dielectric waveguide of length d is represented in the following matrix form of order $2M+4N$:

$$[b] = [S_{\text{LINE}}][a] \tag{A4}$$

where

$$[S_{\text{LINE}}] = \begin{bmatrix} 0_{MM} & 0_{MN} & 0_{MN} & S & 0_{MN} & 0_{MN}\\ 0_{NM} & 0_{NN} & 0_{NN} & 0_{NM} & \tilde{S} & 0_{NN}\\ 0_{NM} & 0_{NN} & 0_{NN} & 0_{NM} & 0_{NN} & \hat{S}\\ S & 0_{MN} & 0_{MN} & 0_{MM} & 0_{MN} & 0_{MN}\\ 0_{NM} & \tilde{S} & 0_{NM} & 0_{NM} & 0_{NN} & 0_{NN}\\ 0_{NM} & 0_{NN} & \hat{S} & 0_{NM} & 0_{NN} & 0_{NN}\end{bmatrix} \tag{A5}$$

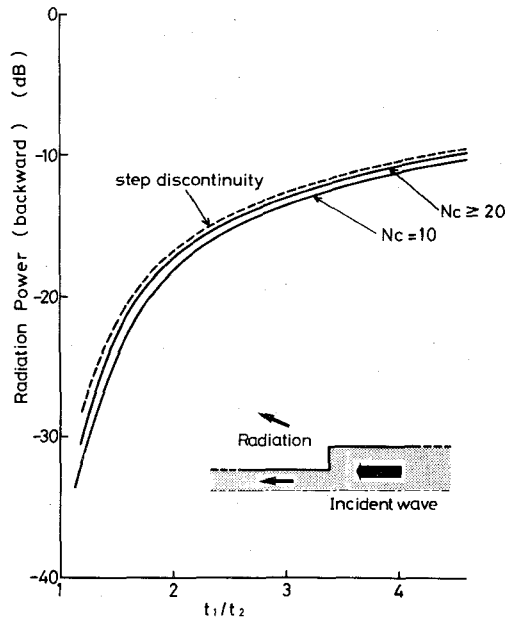

Fig. 15. Maximum backward radiation powers observed within the stopband region. The solid curves are the results obtained by the present method for the periodic structure with a finite number of corrugations N_c, while the dotted curve indicates the radiation power obtained for the step discontinuity shown in the inset.

$[0_{IJ}]$ means the zero matrix of the order $I \times J$ and the superscript t denotes transposition. $[\tilde{S}]$ and $[\hat{S}]$ are matrices of order N, the elements of which are given by (11) and (13), respectively, while $[S]$ is a matrix of the order M corresponding to the surface modes in (3), and its elements S_{mq} are given by

$$S_{mq} = \delta_{mq}\exp(-j\beta_m d). \tag{A8}$$

APPENDIX III

The scattering matrix $[S_{\text{STEP}}]$ for the isolated step discontinuity is expressed as follows:

$$[b] = [S_{\text{STEP}}][a] \tag{A9}$$

where the definitions of $[a]$ and $[b]$ are the same as in (A6) and (A7) with z_1 and z_2 replaced by 0^- and 0^+, respectively.

Let us first consider the case where only the qth surface mode is incident on the step from the left-hand side with amplitude $A_q(0^-) = 1$ and otherwise zero ($A_p(0^-) = 0$ for

$$\begin{aligned}[a] = [&A_0(z_1),\cdots,A_{M-1}(z_1),A_M(z_1),\cdots,A_{M+N-1}(z_1),A_{M+N}(z_1),\\ &\cdots,A_{M+2N-1}(z_1),A_0(z_2),\cdots,A_{M-1}(z_2),A_M(z_2),\cdots,\\ &A_{M+N-1}(z_2),A_{M+N}(z_2),\cdots,A_{M+2N-1}(z_2)]^t\end{aligned} \tag{A6}$$

$$\begin{aligned}[b] = [&B_0(z_1),\cdots,B_{M-1}(z_1),B_M(z_1),\cdots,B_{M+N-1}(z_1),B_{M+N}(z_1),\\ &\cdots,B_{M+2N-1}(z_1),B_0(z_2),\cdots,B_{M-1}(z_2),B_M(z_2),\cdots,\\ &B_{M+N-1}(z_2),B_{M+N}(z_2),\cdots,B_{M+2N-1}(z_2)]^t.\end{aligned} \tag{A7}$$

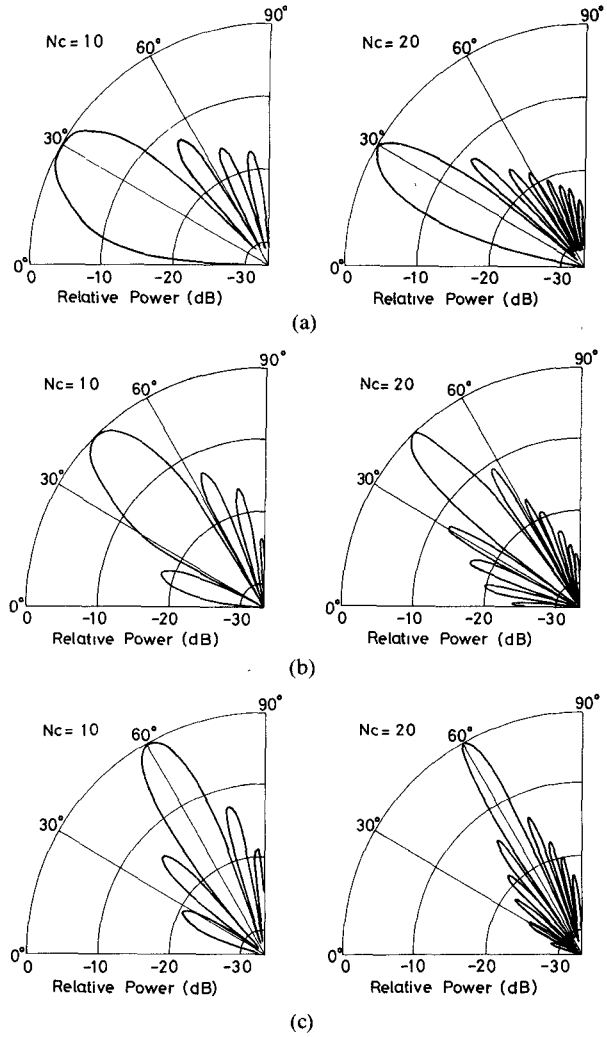

Fig. 16. Backward radiation patterns from the periodic structure with a finite number of corrugations N_c: (a) normalized period $2d/\lambda_0 = 0.477$, (b) $2d/\lambda_0 = 0.516$, and (c) $2d/\lambda_0 = 0.577$.

$p \neq q$ and $A_p(0^+) = 0$ for all p). For this example, we can obtain $(2M+4N)$ elements of S_{pq} $(p = 0,1,\cdots,2M+4N-1)$ on the qth row of $[S_{\text{STEP}}]$ immediately from the coefficients R_{qp} and T_{qp} as follows:

$$S_{pq} = R_{qp} \qquad S_{M+2N+pq} = T_{qp}. \tag{A10}$$

Following the same method for the incidence of each of the other modes from guide I or guide II, all of the matrix elements for the equivalent network shown in Fig. 4 are solved.

Appendix IV

The terminal impedance $\tilde{Z}_n$ of the spectral composite mode in the radiative part of the continuous spectrum $(0 \leqslant \rho \leqslant n_0 k_0)$ can be defined by

$$\tilde{Z}_n \tilde{h}_{yn}(y) = \tilde{e}_{xn}(y) = \int_0^{n_0 k_0} \{\omega\mu_0/\beta(\rho)\}\, \phi_n(\rho) h_y(y,\rho)\, d\rho. \tag{A11}$$

Multiplying both sides by $\tilde{e}_{xn}(y)$ and using the orthonormal relation (A1), we obtain

$$\begin{aligned}\tilde{Z}_n &= \int_{-\infty}^{\infty} \left\{ \int_0^{n_0 k_0} \phi_n(\rho') e_x(y,\rho')\, d\rho' \right\} \cdot \left[\int_0^{n_0 k_0} \{\omega\mu_0/\beta(\rho)\}\, \phi_n(\rho) h_y(y,\rho)\, d\rho \right] dy \\ &= \int_0^{n_0 k_0} \phi_n(\rho') \cdot \left[\int_0^{n_0 k_0} \{\omega\mu_0/\beta(\rho)\}\, \phi_n(\rho) \delta(\rho-\rho')\, d\rho \right] d\rho' \\ &= \int_0^{n_0 k_0} \{\omega\mu_0/\beta(\rho')\}\, \phi_n(\rho') \phi_n(\rho')\, d\rho'. \end{aligned} \tag{A12}$$

In the same way, $\hat{Z}_n$ in the reactive part $(n_0 k_0 \leqslant \rho \leqslant \alpha n_0 k_0)$ is obtained:

$$\hat{Z}_n = -j \int_{n_0 k_0}^{\alpha n_0 k_0} \{\omega\mu_0/\gamma(\rho')\}\, \psi_n(\rho') \psi_n(\rho')\, d\rho'. \tag{A13}$$

References

[1] R. M. Knox and P. P. Toulious, "Integrated circuits for millimeter through optical frequency range," in *Proc. Symp. Submillimeter Waves, MRI* (Polytechnic Institute Brooklyn, New York), Mar. 1970, pp. 497–516.

[2] T. Itoh, "Inverted strip dielectric waveguide for millimeter-wave integrated circuits," *IEEE Trans. Microwave Theory Tech.*, vol. MTT-24, pp. 821–827, Nov. 1976.

[3] H. Shigesawa and M. Tsuji, "Mode propagation through a step discontinuity in dielectric planar waveguide," in *Proc. 1984 IEEE/MTT-S Int. Microwave Symp.* (San Francisco, CA), May 1984, pap. 7–17.

[4] H. Shigesawa and M. Tsuji, "Mode propagation through a step discontinuity in dielectric planar waveguide," *IEEE Trans. Microwave Theory Tech.*, vol. MTT-34, pp. 205–212, Feb. 1986.

[5] D. Marcuse, *Light Transmission Optics*, 2nd ed. New York: Van Nostrand Reinhold, 1982, ch. 8.

[6] R. E. Collin, *Field Theory of Guided Waves*. New York: McGraw-Hill, 1960, ch. 9.

[7] S. F. Mahmoud and J. C. Beal, "Scattering of surface waves at a dielectric discontinuity on a planar waveguide," *IEEE Trans. Microwave Theory Tech.*, vol. MTT-23, pp. 193–198, Feb. 1975.

[8] K. Morishita, S. Inagaki, and N. Kumagai, "Analysis of discontinuities in dielectric waveguides by means of the least squares boundary residual method," *IEEE Trans. Microwave Theory Tech.*, vol. MTT-27, pp. 310–315, Apr. 1979.

[9] T. E. Rozzi and G. H. In'tVeld, "Field and network analysis of interacting step discontinuities in planar dielectric waveguides," *IEEE Trans. Microwave Theory Tech.*, vol. MTT-27, pp. 303–309, Apr. 1979.

[10] H. Shigesawa and M. Tsuji, "A new modal expression of the fields on dielectric waveguides of open type," in *Proc. 1987 URSI Radio Science Meeting* (Blacksburg, VA), June 1987, pap. JB01-5.

[11] D. G. Luenberg, *Optimization by Vector Space Methods*. New York: Wiley, 1969, ch. 3.

[12] A. Sommerfeld, *Partielle Differentialgleichungen der Physik* (translated into Japanese by H. Masuda. Tokyo: Kodansha, 1986).

[13] C. Elachi, "Waves in active and passive periodic structure: A review," *Proc. IEEE*, vol. 64, pp. 1666–1698, Dec. 1976.

[14] D. Kajfez and P. Guilloin, Eds., *Dielectric Resonators*. Dedham, MA: Artech House, 1986, ch. 8.

[15] K. Koshiba, T. Miki, K. Ooishi, and M. Suzuki, "On finite element solutions of the discontinuity problem in a bounded dielectric slab waveguide," *Trans. IECE Japan*, vol. E66, pp. 250–251, Apr. 1983.

[16] T. Hosono, T. Hinata, and A. Inoue, "Numerical analysis of the discontinuities in slab dielectric waveguides," *Radio Sci.*, vol. 17, pp. 75–83, Jan.–Feb. 1982.

[17] M. Tsuji and H. Shigesawa, "Mutual interference between the guided wave and the leaky wave regions and its effects on the performance of dielectric grating filters," in *Proc. 1986 IEEE/MTT-S Int. Microwave Symp.* (Baltimore, MD), June 1986, pap. B-5.

[18] M. Tsuji, H. Shigesawa, and A. A. Oliner, "Microwave network design approach to dielectric periodic leaky-wave antennas," in

Proc. 1986 IEEE/APS Int. Antenna Propagat. Symp. (Philadelphia, PA), June 1986, pap. AP05.

[19] M. Tsuji, H. Shigesawa, and A. A. Oliner, "Microwave network approach to dielectric periodic leaky-wave antennas," in *Proc. 1985 Int. Symp. Antennas Propagat.* (Kyoto, Japan), Aug. 1985, pap. 022-5.

[20] M. Tsuji and H. Shigesawa, "Wave scattering from a dielectric periodic grating with finite extent," in *Proc. URSI National Radio Science Meeting* (Philadelphia, PA), June 1986, pap. UB15-3.

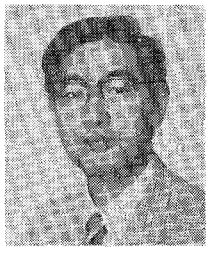

Hiroshi Shigesawa (S'62–M'63–SM'85) was born in Hyogo, Japan, on January 5, 1939. He received the B.S., M.S., and Ph.D. degrees in electrical engineering from Doshisha University, Kyoto, Japan, in 1961, 1963, and 1969, respectively.

Since 1963, he has been with Doshisha University. From 1979 to 1980, he was a Visiting Scholar at the Microwave Research Institute, Polytechnic Institute of New York, Brooklyn, NY. Currently, he is a professor in the Faculty of Engineering, Doshisha University. His present research activities involve millimeter- and submillimeter-wave guiding structures and devices and scattering problems of electromagnetic waves.

Dr. Shigesawa is a member of the Institute of Electronics, Information and Communication Engineers (IEICE) of Japan, the Institute of Electrical Engineers (IEE) of Japan, and the Optical Society of America (OSA).

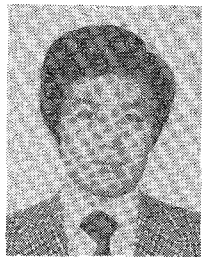

Mikio Tsuji (S'77–M'82) was born in Kyoto, Japan, on September 10, 1953. He received the B.S., M.S., and Ph.D. degrees in electrical engineering from Doshisha University, Kyoto, Japan, in 1976, 1978, and 1985, respectively.

Since 1981, he has been with Doshisha University, where he is now an assistant professor. His research activities have been concerned with millimeter- and submillimeter-wave guiding structures and devices.

Dr. Tsuji is a member of the Institute of Electronics, Information and Communication (IEICE) of Japan.